Conditions for forming composite carbon nanotube-diamond like carbon material that retain the good properties of both materials

Wei Ren, Ajai Iyer, Jari Koskinen, Antti Kaskela, Esko I. Kauppinen, Konstantin Avchaciov, and Kai Nordlund

Citation: Journal of Applied Physics **118**, 194306 (2015); doi: 10.1063/1.4935820
View online: http://dx.doi.org/10.1063/1.4935820
View Table of Contents: http://scitation.aip.org/content/aip/journal/jap/118/19?ver=pdfcov
Published by the AIP Publishing

Conditions for forming composite carbon nanotube-diamond like carbon material that retain the good properties of both materials

Wei Ren,[1,a)] Ajai Iyer,[2] Jari Koskinen,[2] Antti Kaskela,[3] Esko I. Kauppinen,[3] Konstantin Avchaciov,[1] and Kai Nordlund[1]
[1]*Department of Physics, University of Helsinki, P.O. Box 43, FIN-00014 Helsinki, Finland*
[2]*Department of Materials Science and Engineering, School of Chemical Technology, Aalto University, P.O. Box 16200, 00076 Espoo, Finland*
[3]*NanoMaterials Group, Department of Applied Physics, Aalto University School of Science, P.O. Box 15100, 00076 Aalto, Finland*

(Received 20 July 2015; accepted 3 November 2015; published online 20 November 2015)

Carbon nanotubes are of wide interest due to their excellent properties such as tensile strength and electrical and thermal conductivity, but are not, when placed alone on a substrate, well resistant to mechanical wear. Diamond-like carbon (DLC), on the other hand, is widely used in applications due to its very good wear resistance. Combining the two materials could provide a very durable pure carbon nanomaterial enabling to benefit from the best properties of both carbon allotropes. However, the synthesis of high-quality diamond-like carbon uses energetic plasmas, which can damage the nanotubes. From previous works it is neither clear whether the quality of the tubes remains good after DLC deposition, nor whether the DLC above the tubes retains the high sp^3 bonding fraction. In this work, we use experiments and classical molecular dynamics simulations to study the mechanisms of DLC formation on various carbon nanotube compositions. The results show that high-sp^3-content DLC can be formed provided the deposition conditions allow for sideways pressure to form from a substrate close beneath the tubes. Under optimal DLC formation energies of around 40–70 eV, the top two nanotube atom layers are fully destroyed by the plasma deposition, but layers below this can retain their structural integrity. © *2015 AIP Publishing LLC*. [http://dx.doi.org/10.1063/1.4935820]

I. INTRODUCTION

Single-walled carbon nanotubes (SWCNTs) and their networks are promised as materials which have potential applications as optically transparent conductive electrodes, thin-film field transistors and sensors,[1] due to their unique electrical conductivity and optical transparency.[2] However, the SWCNT-networks cannot resist mechanical damage from scratching and wear,[3] which makes them challenging to use in mechanical applications. It has been reported that a carbon coating could improve the mechanical properties of the SWCNT networks, i.e., improved elasticity and better nanowear resistance.[4]

By using vacuum arc discharge, fully ionized carbon plasma with controllable energy and flux are deposited on the nanostructures, where amorphous diamond-like carbon (DLC) has been reported to grow on top, resulting in enhanced mechanical strength.[5–10] In DLC films, carbon atoms are bonded together mainly in the form of sp^2 and sp^3 hybridizations. Because DLC films are well known for their high hardness and high elastic modulus, they are utilized in a wide range of applications to improve properties such as high wear resistance, chemical inertness, high electrical resistivity, and low friction coefficients.[11] This has led to practical applications such as antireflective and scratch-resistant wear-protective coating for IR optics,[12,13] wear and corrosion protection of magnetic storage media,[14] and coating and protecting biological implants against corrosion as diffusion barriers.[15,16] DLC-CNT composites could be formed by doing vacuum arc deposition on CNTs with an average energy of carbon ions about 30–70 eV. The functional SWCNT-networks could then be covered by the amorphous DLC matrix, while the electrical conductivity and optical transparency are preserved with enhanced mechanical properties.[4]

It is still challenging to characterize the structure of DLC films because of their complicated amorphous morphology. There are some experimental techniques for characterization of DLC, for example, Fourier transform infrared spectroscopy (FTIR), high resolution nuclear magnetic resolution (NMR), electron energy loss spectroscopy (EELS), X-Ray Photoelectron Spectroscopy (XPS), Auger spectroscopy, etc. It also has been reported that by either thermal activation[17,18] or low energetic ion irradiations,[19] the structure of the metastable DLC materials will convert some sp^3 bonds to sp^2 bonds towards graphite-like carbon.[11] Thus a fundamental understanding of carbon hybridization under low energetic carbon atom bombardments is of great interest. In this paper, experimental details of SWCNT network synthesis and amorphous carbon deposition on it are given. The sp^2 and sp^3 hybridizations are quantized by XPS. Classical molecular dynamics (MDs) simulations were performed to examine ion beam depositions of such DLC films on SWCNTs, carbon foams, multiwalled carbon nanotubes (MWCNTs) SWCNT bundles, with and without diamond substrates, as well as temperature effects on DLC films growth. The atomic structures of

[a)]Email: wei.ren@helsinki.fi

the growing films were analyzed to examine the quality of DLC films by quantifying the ratios of sp^2 and sp^3 bondings.

II. EXPERIMENTAL METHOD

SWCNTs were synthesized by a high temperature floating catalyst CVD process, based on thermal decomposition of ferrocene to form iron nanoparticles.[20–22] Following this catalytic decomposition of carbon monoxide via Bouduard reaction on the iron nanoparticle surfaces leads to nucleation and growth of SWCNTs in gas phase, inside a quartz walled laminar flow reactor, maintained at 880 °C based on previous optimization.[20] The SWCNTs can aggregate in gas phase forming bundles, consisting of several parallel SWCNTs due to surface energy minimization.[23] SWCNTs were collected on nitrocellulose membrane filters (Millipore Ltd. HAWP, 0.45 μm pore size) at the outlet of the reactor to form randomly oriented SWCNT networks. These SWCNT networks are subsequently transferred onto Si substrates using a room temperature press transfer method described in detail elsewhere.[22,24]

Tetrahedral amorphous carbon (ta-C) coating was deposited onto the press transferred SWCNT networks using a pulsed Filtered Cathodic Vacuum Arc (p-FCVA) deposition system at Aalto University. A pulse forming network, charged to 400 V (pulse current 650 A) was used to strike the triggerless arc[25] with a frequency of 1 Hz and a knee filter with 45° bend was utilized to filter out macro-particles. The working pressure during depositions was 2×10^{-6} Torr and the substrates were at floating potential and room temperature (300 K). The cathode to substrate distance was maintained at 110 mm and substrates were rotated to ensure homogeneous film deposition. The deposition rate of the ta-C coating was around 0.1 nm/pulse (on silicon), for a cathode to substrate distance of 110 mm, as measured by a contact profilometer (Dektak 6 M). 20 nm thick ta-C coating was deposited onto Si substrates (reference sample) and on the SWCNT networks (test sample).

XPS was performed by an Axis Ultra electron spectrometer (Kratos Analytical) using monochromatic Aluminium Kα (E = 1487 eV) irradiation. Low resolution survey scans were recorded in hybrid mode, together with high resolution C1s spectra using 5 eV pass energy and 50 meV energy step with X-Ray power of 150 W. In all XPS measurements the area of analysis was 700 μm × 300 μm.

These experimental observations clearly show that high-sp^3 content DLC can be formed on carbon nanotube networks. However, the mechanism is not obvious. Previous work on DLC formation[26–28] has explained the formation of the DLC to be due to a "subplantation" effect, i.e., that the carbon atoms stop inside a material where a transient high pressure and temperature can promote formation of high sp^3 fractions. However, the density of the nanotubes is very low, and hence it is not a priori clear how a high sp^3 content can be produced when the carbon is landing on top of them. To understand how and under which conditions the DLC can be formed, we utilize here MDs computer simulations of DLC deposition on various carbon nanotube morphologies.

III. EXPERIMENTAL RESULTS

SWCNT samples were imaged by S-4700 (Hitachi) Scanning Electron Microscopy (SEM) pre (Fig. 1(a)) and post (Fig. 1(b)) ta-C deposition. Image analysis, using ImageJ software shows areal coverage density of SWCNTs on the substrate is an average of 40%. Post deposition, the presence of coating thickens individual SWCNT bundle and network morphology, is different in comparison to an un-coated network (Fig. 1(a)).

Fig. 2 shows the XPS C1s high resolution spectra for un-coated SWCNTs, ta-C reference sample, and ta-C coated SWCNT sample with curve fitting for different components. The C1s spectrum for un-coated SWCNTs only (Fig. 2(a)) was fitted with an asymmetric Doniach-Sunjic[33] profile after removal of Shirley background, to fit conductive sp^2 bonded carbon due to its semi-metallic behavior[34] and a Gaussian component. The Doniach-Sunjic fit peak at 284.4 eV is identified as sp^2 bonded carbon[35–38] and the uncoated SWCNTN has a dominant sp^2 carbon bonding fraction (around 82% of C1s spectrum area). The Gaussian component at 285.5 eV is attributed to defects in the nanotube structure as shown in literature[39,40] and minor surface contamination.

The C1s spectra for reference ta-C sample (Fig. 2(b)) and ta-C coated SWCNT sample (Fig. 2(c)) were fitted with

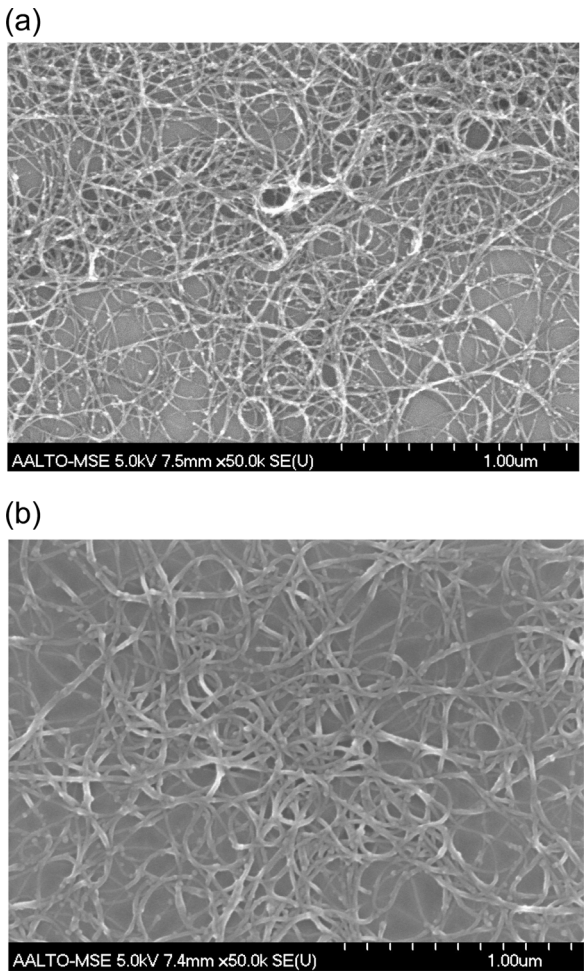

FIG. 1. SEM image of SWCNT bundles (a) pre-deposition; (b) post deposition of 20 nm taC.

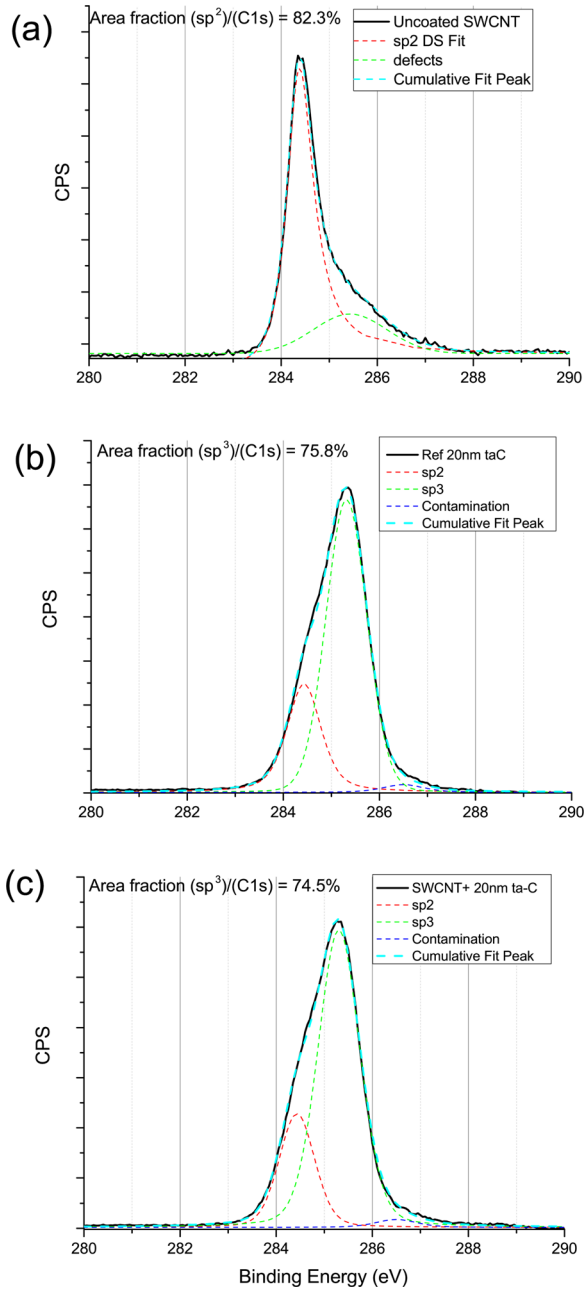

FIG. 2. XPS high resolution C1s spectra with peak fits; (a) Un-coated SWCNTs with 82% sp^2 bonding fraction; (b) 20 nm thick reference ta-C coating with 76% sp^3 bonding fraction; (c) SWCNT network with 20 nm thick ta-C deposited showing 75% sp^3 bonding fraction.

mixed Gaussian-Lorentian components after removal of Shirley background. The sp^2 component in ta-C coating is not fitted by the Doniach-Sunjic component as the sp^2 phase is disordered and ta-C is insulating in nature.[35] The reference ta-C spectrum (Fig. 2(b)) has primary peaks at 284.4 eV and 285.3 eV corresponding to sp^2 and sp^3 bonded carbon, respectively, and a secondary peak at 286.5 eV, attributed to C-O contamination, due to air exposure. The peak fits match well with similar studies in literature[35–38] and show a significant sp^3 bonding fraction (around 76% of C1s spectrum area). Comparing the reference ta-C (Fig. 2(b)) and ta-C coated SWCNTs (Fig. 2(c)) spectra we observe no significant difference in either spectral shape or fitted peak positions. The ta-C coated SWCNT sample also shows a significant sp^3 bonding fraction (around 75% of C1s spectrum area), similar to reference ta-C sample. This indicates that the coating on the SWCNT network is good quality ta-C.

IV. SIMULATION METHOD

The deposition processes were simulated by using the classical MD method with the PARCAS code.[29,44–46] For modelling the C-C interactions, the analytic bond-order potential of Brenner[30] with extended cutoff parameters was used. The original form of the cut-off function, which describes the range of the local atomic orbitals, was only limited to the first neighbors with the cutoff parameters ($R = 1.7$ Å, $S = 2.0$ Å),[30,31] which allows the existence of compressed graphite structures with even higher densities than the diamond.[28] It has been reported by Jäger and Albe[28] that by adjusting the cutoff parameters to $R = 1.95$ Å and $S = 2.25$ Å much higher sp^3 fractions could be achieved.

The quality of the deposited films were analysed by the coordination numbers, which were calculated by the radial distribution function (RDF) within the first cutoff length of 1.9 Å. The threefold atoms were considered as sp^2 hybridization, while the fourfold atoms were considered as sp^3 hybridization. Meanwhile, depth profiles were calculated with the depth interval of 2.05 Å, indicating the dependence of DLC quality on the deposition depths. Mass densities were also calculated compared to pure diamond and graphite. Furthermore, the overall RDF, and the RDF calculated only at sp^2 or sp^3 sites with the contributions of sp^2 and sp^3 coordinated neighbours, were compared to study the short range order of the deposited films. Ring analysis[32] was applied to quantify the overall disorder of the grown films.

A diamond {111} substrate with a box size of about (30, 30, 20) Å was used as the substrate. Periodic boundary conditions were used at the lateral directions of the diamond substrate, while the top surface was kept open. To prevent the entire system from moving during the irradiation, two atomic layers were fixed at the bottom. The incoming carbon atoms with the energies of 30, 40, 50, and 70 eV bombarded perpendicular to the open surface. A random cell shift in the lateral direction was used for each ion bombardment with periodic boundary conditions. The entire deposition process was simulated at 100 K and 300 K or at temperatures of 100–1000 K in one case. During each bombardment within the time scale of 15 ps, the heat dissipation from the impact region to the rest of the system was modelled by Berendsen temperature scaling,[41] by which the periodic boundaries within a thickness of 7 Å were immersed in a heat bath at 100 K and 300 K. A relaxation time of 5 ps between every two impacts was used to linearly cool down the entire system to 100 K and 300 K.

A. The effect of electronic stopping power

Electronic stopping refers to the slowing down process of a projectile ion because of the inelastic collisions between bound electrons and the energetic ion. When the impacting energy is high, the ion is slowed down mainly by electronic stopping.[46] To test whether the electronic stopping power

affected the structures of the deposited films or not, the simulations of deposition processes with and without electronic stopping power were simulated and compared. We found that the sp^3 hybridizations did not change too much whether the electronic stopping power was involved or not. Hence we conclude that the electronic stopping power does not play an important role on the bonding structures of carbon hybridizations. According to a SRIM[42] calculation, at low injecting carbon energy below 100 eV to diamond carbon, the electronic stopping power was about 13% of the total electronic and nuclear stopping powers.

We first carried out simulations of C deposition on a pristine diamond (with no nanotube on top) to get a point of comparison with the NT systems. Fig. 3 shows the simulation results on a pristine diamond with deposition energy of 70 eV at 100 K and 300 K, without electronic stopping power. The negative deposition depth is the growing direction, and the positive depth of the substrate with the interface at 0 Å. At both temperatures, the sp^3 fractions went down from 100% to very low values at the surface of the growing films. It is shown that at 100 K the fractions of sp^3 hybridizations decreased at the near diamond grown layers from 100% to 45% gradually within the depth of 20 Å, while at

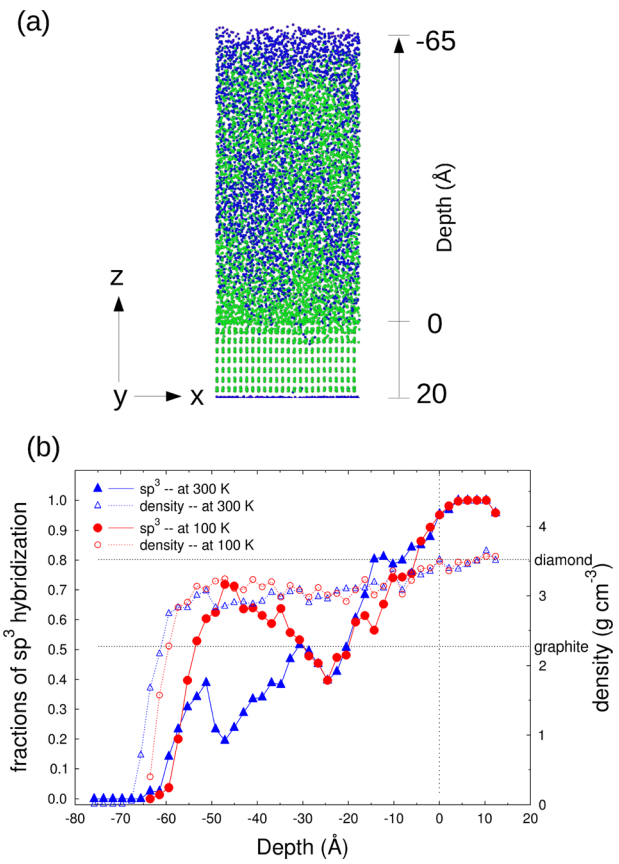

FIG. 3. (a) Schematic sketch of the simulation cell after about 9000 impacts at 100 K with energy of 70 eV. (b) Depth profiles of sp^3 fraction (left-hand) and mass density (right-hand) of the deposited films on diamond {111} substrate without electronic stopping power, at 100 K and 300 K. The deposition direction is to the negative depth value, while the diamond surface is at 0 Å. Approximately 9000 impacts with energy of 70 eV bombarded on the cell size of (30, 30, 20) Å of pure diamond, with the final depth of the deposited film about 60 Å, which corresponds to about 30 atomic layers of the ideal diamond {111} structure.

further deposition beyond the depth of 20 Å the fractions increased to more stable values at about 60%–70%. Meanwhile, at the temperature of 300 K at the very near diamond substrate with the thickness of 20 Å, the fractions of four-fold coordinated atoms were kept stable at ~80% indicating a very good DLC quality. However, when the thickness of the growing films was increasing to more than 20 Å, the sp^3 fractions decreased to the values between 30% and 50% and finally vanished to 0 at the surface. At the same time, the mass densities at the inner stable region of the deposited films are about 3.14 g/cm^3 at 100 K and 3.02 g/cm^3 at 300 K, lying closer to the density of diamond (3.52 g/cm^3) than graphite (2.09–2.27 g/cm^3).

B. Radial distribution function

To study the short order of the grown amorphous film, RDF was calculated for two samples with 37.2% and 48.4% sp^3 coordinated atoms excluding the diamond substrate as shown in Fig. 4. The top panel shows the overall RDF for all the atoms, as well as the contributions of sp^2 and sp^3 neighbours. The lower panel explains the RDF calculated only at sp^2 sites with the corresponding sp^2 and sp^3 contributions, and the RDF calculated only at sp^3 sites. It can be seen that for the case of 48.4% sp^3 film, the sp^2 and sp^3 neighbours made the same amount of contributions at the first peak of the overall RDF, which was corresponding to the same percentages of sp^2 and sp^3 coordinated atoms. However, when calculated only at sp^2 sites compared to the overall RDF, the contribution of sp^2 neighbours shows a big increase, while the contribution of sp^3 neighbours also increased comparatively when calculated only at sp^3 sites. This interesting feature can be explained by the separation of sp^2 and sp^3 sites. In other words, sp^3 sites tend to grow close to the diamond substrate, while sp^2 sites were mostly near the surface due to the lack of atoms to form bondings at the top.

C. Ring analysis

To characterize the amorphous films and quantify the overall disorder, ring analysis[32] was used to study the films with varied densities and sp^3 hybridizations grown at different deposition energies. This method analyses the number of prime rings, which were defined in Ref. 32 as rings without any shortcut. The diamond substrates and the surfaces with a thickness of 20 Å were not included in the studied films. As shown in Fig. 5, the films with lower densities and lower sp^3 coordination reveal a relatively more disordered ring analysis when compared to the film with a higher 3.11 g/cm^3 density and 58.2% sp^3 coordination. The more ordered of ring analysis of this film approaches more closely to the ideal diamond structure, where a six-membered ring is the only prime ring configuration.

V. SIMULATION RESULTS

To determine the atomic structures of the deposited films, we simulated the impinging carbon atoms bombarding the SWCNT with a diamond substrate, nano foam with a diamond substrate, suspended SWCNT bundle, and MWCNTs,

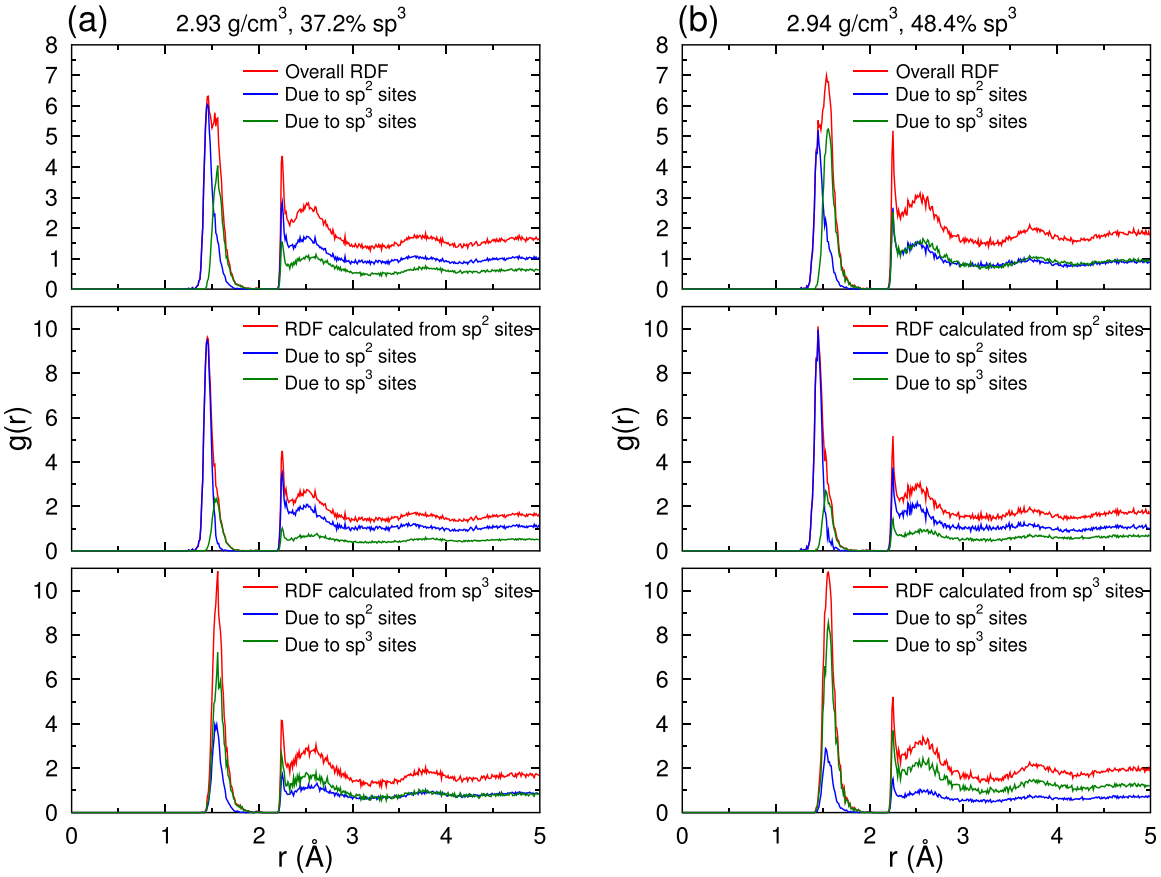

FIG. 4. (a) and (b) Radial distribution function (RDF) g(r) for the two sample films with 37.2% and 48.4% sp^3 coordinated atoms, excluding the diamond substrates at room temperature. The first panels are the overall RDFs calculated for all the atoms, where the contributions of sp^2 and sp^3 neighbours are shown separately. The second and third panels are the RDFs calculated only at sp^2 sites and sp^3 sites, respectively, as well as their corresponding contributions from the sp^2 and sp^3 neighbours. The second peaks in all the RDF plots locate at 2.25 Å which are the artificial peaks due to the cutoff parameters in the potential (see Section III).

as well as MWCNTs with a diamond substrate, as presented in Figs. 6(a)–6(e). For the systems in Figs. 6(a), 6(b), and 6(e), periodic boundary conditions were applied on the two lateral directions of the diamond substrate, including the direction of the tubes or the foam length.

In Fig. 6(a), the chosen CNT with the length of about 26 Å consisting of 450 atoms, was a zigzag SWCNT with the chiral index of (19,0), which gave the diameter of about 15 Å. Meanwhile, the size of the diamond substrate was about (30, 26, 12) Å, which consisted of about 6 atomic layers of the ideal diamond {111}. Before the irradiation, the system was built by connecting the tube on the middle surface of the diamond {111} cell with a distance of 2.0 Å in between, followed by a relaxation at 100 K and 300 K for 100 ps.

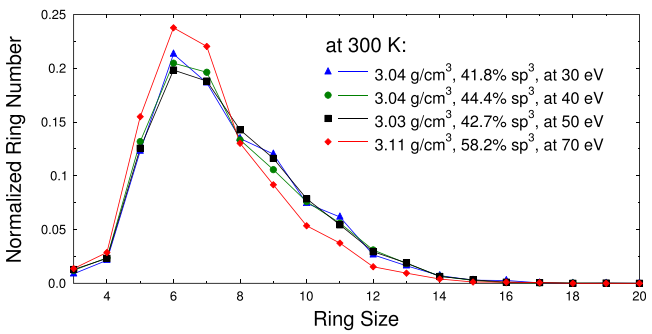

FIG. 5. Ring analysis of the four films with varied densities and sp^3 hybridizations which were growing at room temperature at different deposition energies.

In Fig. 6(b), a nano foam which had a similar size as the CNT (Fig. 6(a)) but with the same density as graphite, is shown. The nano foam was formed by amorphous carbon with the mass density of 2.09 g/cm^3 with a slow annealing from 5000 K to 100 K and 300 K over 1 ns. Then the nano foam with the size of (15.0, 15.0, 30.6) Å consisting of 721 atoms was connected on top of the diamond with a distance of 2.0 Å in between, followed by a relaxation for 1 ns at 100 K and 300 K.

The deposition processes on the SWCNT bundles and MWCNTs with carbon ion energies of 40, 50, 70 eV were also studied, visualized in Figs. 6(c) and 6(d). In Fig. 6(c), the SWCNT bundles consisting of 11704 atoms were obtained by connecting 7 zigzag (19,0) SWCNTs together with the distance of 3.4 Å between each other at the sides. In Fig. 6(d), the MWCNTs composed of (5,5), (10,10), (15,15) armchair SWCNTs, gave the diameter of 6.8 Å, 13.6 Å, and 20.3 Å, with the inter-shell distance of 3.4 Å. The lengths of the bundle and the MWCNTs were about 100 Å at the periodic boundary condition, within which the middle parts of

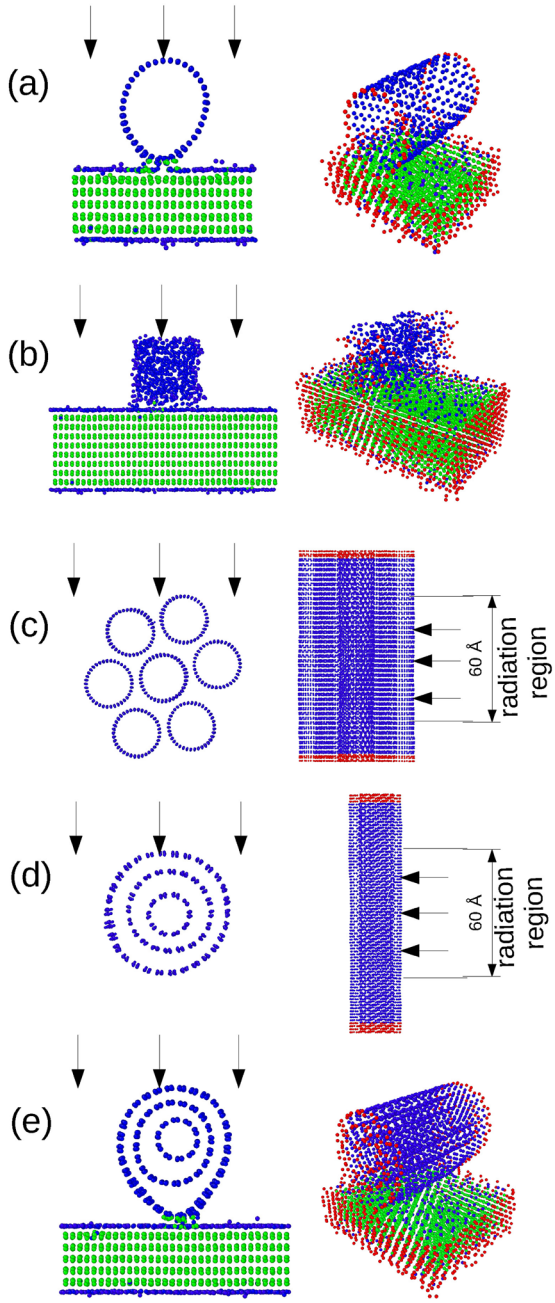

FIG. 6. (a) and (b) Front views and three-dimensional views of the deposited system of the SWCNT and nano foam on the top of the diamond {111} substrate before carbon ion irradiations. (c) and (d) The cross sections and side views of the SWCNT bundle and MWCNTs after relaxation. (e) Front view and three-dimensional view of the deposited system of MWCNTs on the top of the diamond {111} substrate before irradiation. The periodic boundaries in the three-dimensional views and side views are marked with red atoms.

60 Å were the irradiated regions, while at both ends the regions with a thickness of 15 Å were coupled to a heat bath at 100 K and 300 K to dissipate the heat from the impact regions. The tubes were suspended with 2 Å thick layers fixed at both ends.

To test the idea that sidewards pressure is crucial for building up sp^3 configurations, the same MWCNT system on top of the diamond {111} substrate with 6 ideal atomic layers was also used to grow the films on. The visualization of the system is in Fig. 6(e).

A. Deposition on SWCNT with diamond substrate

We found that at the low energy of 40 eV, the structure of the SWCNT can still be identified under such irradiations, with only the top two atomic layers of the diamond substrate damaged. Meanwhile, as the impact energy went higher to 70 eV, the SWCNT was completely destroyed together with the damaged top four atomic diamond substrate layers. The overall RDF of the deposited films of each case illustrated quite well the contribution amounts of sp^2 and sp^3 neighbours, where the higher fraction of sp^3 hybridization resulted in a higher contribution of sp^3 neighbours at the first peak of the overall RDF.

The depth profiles for the fractions of sp^3 hybridization and mass density at 100 K and 300 K were calculated in Fig. 7(f), where a CNT region, a stable inner film region, and a surface region can be clearly identified. In the CNT region, at the energy of 70 eV the structure of the three-fold coordinated SWCNT was completely damaged and transformed to four-fold coordination, while at 40 eV the structure at this region was still identified as three-fold hybridization. Hence, the fractions of sp^3 bonded atoms at 70 eV was relatively higher than those at 40 eV, where the fractions were 0%–10% in the CNT region. In the inner films, the fractions of sp^3 hybridization became stable, lying at about 50%–60% at 100 K, and 30%–55% at 300 K, which were quite close to those directly deposited on the pure diamond substrate. At the surface region, the sp^3 fractions decreased to 0 due to the domination of the sp^2 bonded atoms. Hence, at the beginning of the deposition, the sp^3 bondings were hardly constructed because of the existence of the CNT, while when the films were further deposited to a stable level, significant percentages of the sp^3 configurations would be created. Meanwhile, the mass density of the stable inner film was again lying in the middle of the densities of diamond and graphite. Fig. 7(g) shows the result of ring analysis studied on the obtained samples at 100 K and 300 K. When compared with other films, the sample with irradiation energy of 40 eV at 100 K, which had the highest density of 3.10 g/cm^3 and highest sp^3 fraction of 52.7%, showed the most oriented order ring analysis with the most common ring configurations being six-ring and seven-ring sizes.

To illustrate the temperature effect on sp^3 hybridization, the deposition processes were simulated with the irradiation energy of 30 eV at temperatures of 100, 300, 600, 800, and 1000 K, as described in Fig. 8. It can be seen that at lower temperatures the DLC quality was relatively better than those at higher temperatures. When the temperature increased from 100 K to 300 K, the sp^3 fraction decreased from 40%–60% to 25%–40%, while at higher temperatures of 600, 800, and 1000 K, the sp^3 fractions dropped below 5% leaving the pre-dominating sp^2 hybridizations. The low sp^3 bondings could be explained by the thermal relaxation which reconfigured the sp^3 bondings to energetically more favorable sp^2 bondings. This temperature dependence agrees qualitatively with the experimental observations of Koskinen[43] who reported a transition temperature of about 400 °C, above which the sp^2 configurations were pre-dominated during the deposition process.

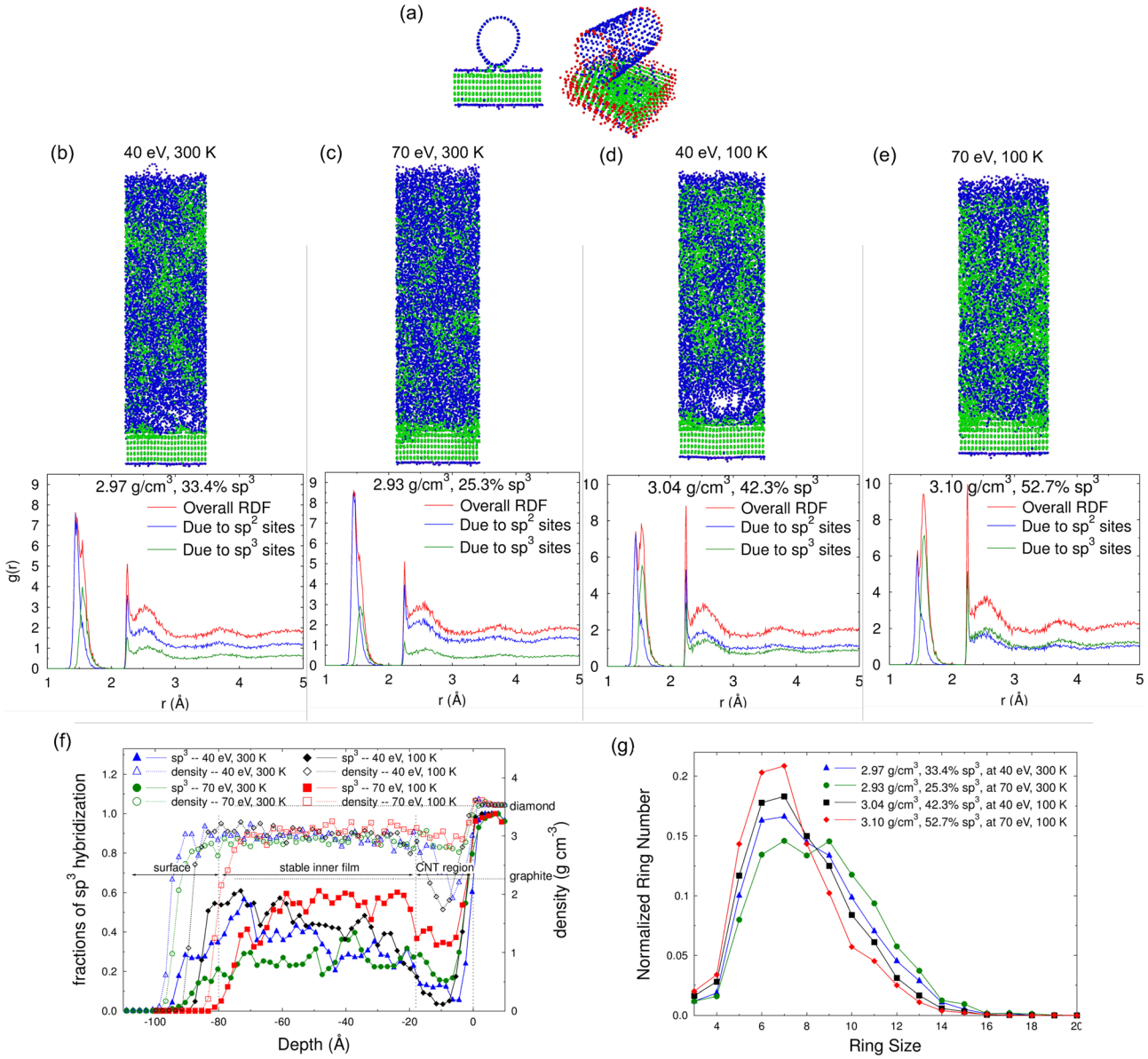

FIG. 7. (a) Front view and three-dimensional view of the deposited system of the SWCNT on the top of the diamond {111} substrate before carbon ion irradiations. (b)–(e) The first panels are the visualizations of the composited films on the deposited systems at 100 K and 300 K with the irradiating energies of 40 eV and 70 eV, respectively, after about 10 000 irradiations. The blue atoms stand for sp^2 bonded atoms, while the green atoms stand for sp^3 bonded atoms. The second panels are the overall RDFs and its sp^2 and sp^3 contributions of the corresponding grown films, calculated at all atoms of the deposited films only which exclude the atoms of the diamond substrates. (f) Depth profiles of sp^3 fractions and mass density of the deposited films. The vertical dashed lines mark the CNT region, the stable inner film region, and the surface region. (g) Ring analysis of the four deposited films which exclude the atoms of the diamond substrates.

B. Deposition on carbon foam with a diamond substrate

The same method as for the SWCNT was used to simulate the deposition processes with the impacting energies of 40 eV and 70 eV. We found that sp^3 fractions at 100 K (up to ~55% at 70 eV) were relatively higher than those at 300 K (~40% at 70 eV) at the inner stable film region. Ring analysis shows more six-ring ordered rings with the higher sp^3 fractions.

C. Deposition on SWCNT bundle

The fractions of the sp^3 configurations for the deposited films on the SWCNT bundles were also calculated. However, only a small amount of sp^3 bondings could be observed from

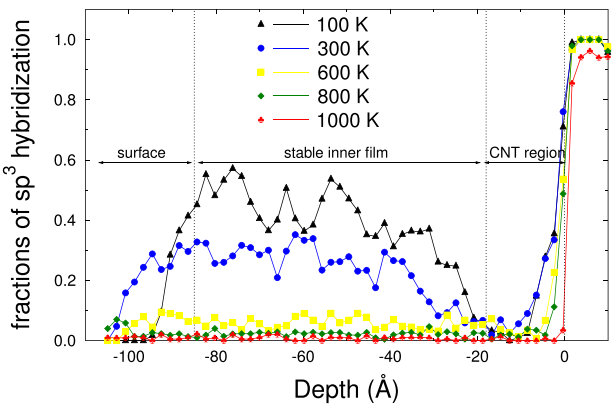

FIG. 8. Depth profiles of sp^3 fractions of the deposited films on SWCNT on top of the diamond {111} substrate with the deposition energy of 30 eV, at 100, 300, 600, 800, and 1000 K, respectively.

the pure sp^2 system at both temperatures. At the low irradiation energy, the top CNTs survived and stayed almost intact, while at the energy of 70 eV the carbon atoms penetrated into 1–2 CNTs and started to grow inside the tubes. The lack of side pressure, due to the suspension at both ends of the bundle, as well as the curvature of the bundle surface, would be the possible reasons causing the low sp^3 fractions.

D. Deposition on MWCNTs

We found that at the irradiation energy of 40 eV, only the outermost shell was damaged and the incoming carbon atoms started to grow on top of the substrate, leaving the 2 inner shells structurally and functionally intact. Meanwhile, at the energy of 50 eV, the impacts penetrated into the two outer shells and the atoms started to fill the space between the shells, while the top half of the MWCNT was completely destroyed at the energy of 70 eV. By analysing the depth profiles of sp^3 fractions of the growing films, we found that the sp^3 fractions of the deposited films at both 100 K and 300 K were still very low, compared to the pure sp^2 system.

E. Deposition on MWCNTs with a diamond substrate

Visualization of the structures of the system and the growing films with the deposition energy of 50 eV and 70 eV at 100 K and 300 K is shown in Figs. 9(a)–9(e). It can be seen that at 50 eV the inner two tubes stayed almost intact embedded in the grown films, while at 70 eV the innermost tube and the lower half part of the MWCNT can survive at

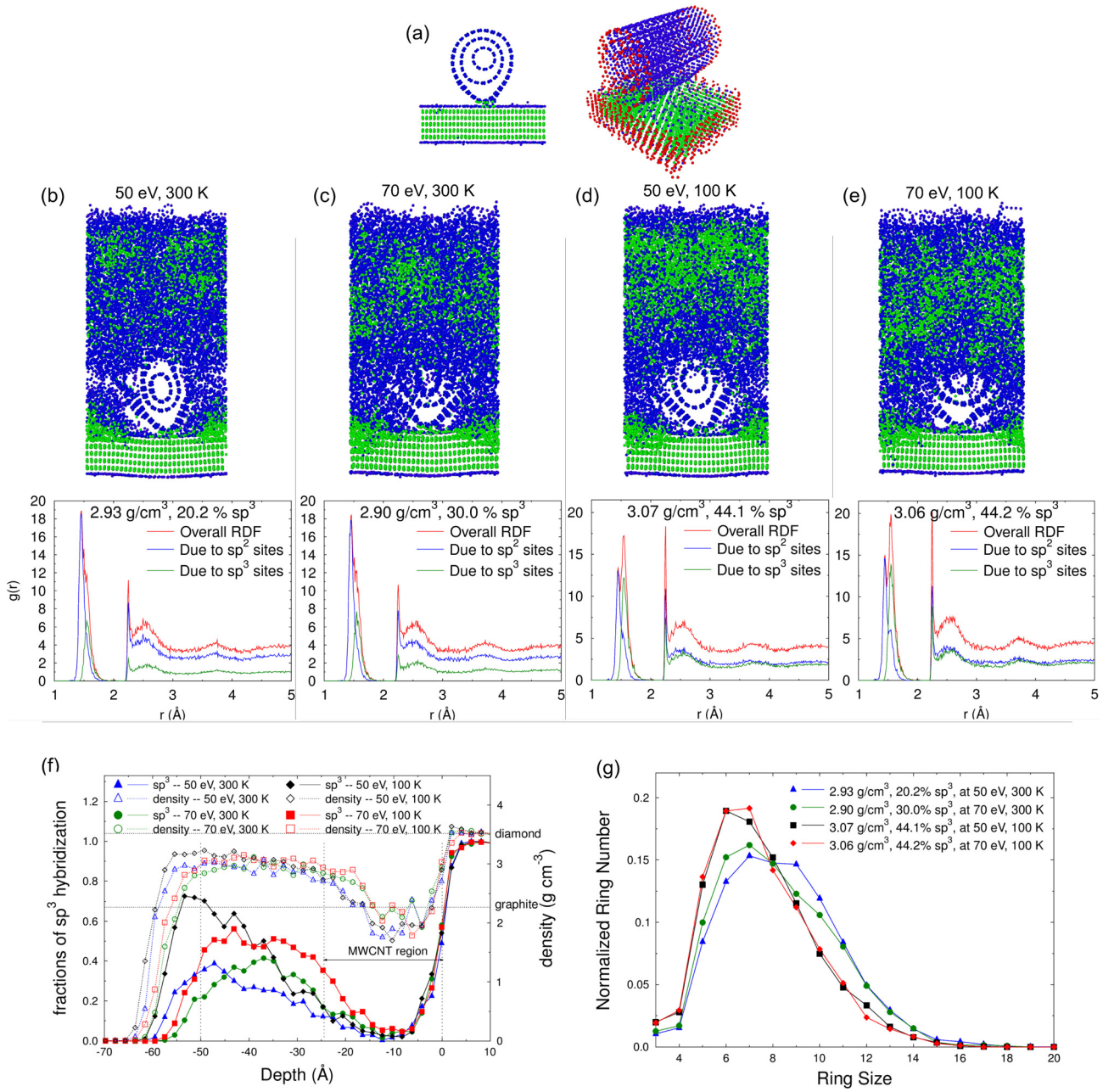

FIG. 9. (a) Front view and three-dimensional view of the deposited system of MWCNTs on the top of the diamond {111} substrate before irradiation. (b)–(e) The visualization of the composited films at 100 K and 300 K with energies of 50 eV and 70 eV, respectively, after about 10 000 impacts, and the corresponding overall RDFs with its sp^2 and sp^3 contributions. (f) Depth profiles of sp^3 fractions and mass density of the deposited films. (g) Ring analysis of the deposited films.

both temperatures. As usual, the overall RDF, as well as the densities and sp^3 fractions of each corresponding films are also presented, illustrating that at the first peak of the overall RDF, the contribution of the sp^3 coordinated neighbours was proportional to the overall sp^3 fraction and the density of the studied film. By analysing the depth profiles of sp^3 fractions of the growing films in Fig. 9(f), we found that the depth of the MWCNT region was about (−25, 0) Å, where sp^3 hybridizations were barely observed because of the curvature of the MWCNT. However, beyond this region, the sp^3 fractions increased gradually to more stable values. For example, at 100 K with 50 eV, the sp^3 fraction continuously increased to ∼75% with the increasing grown depth, indicating very good DLC quality. The sp^3 fraction at 300 K went stable up to 40% in the inner stable film region. Again in Fig. 9(g), the higher fractions of the six-ring illustrated the higher sp^3 hybridization and higher density.

VI. DISCUSSION

We have studied the structural configurations of sp^2 and sp^3 bondings of vacuum arc deposition on carbon nano hybrid materials with experiments and MD simulations. The experimental results show that high quality ta-C can be formed on SWCNT bundles on Silicon substrate. From the MD simulation results of deposition on the SWCNT bundle and MWCNTs without diamond substrate, we found that only a small amount of sp^3 bondings were observed due to the fact that there was no sideward confinement, and that the curvature of the CNTs made sp^3 bonding creation difficult. For the cases with diamond {111} substrates, like pure diamond, SWCNT, nano foam as well as MWCNT, at 100 K DLC films of good quality could be obtained at the inner stable films where the sp^3 fractions can reach up to 70% with 70 eV irradiation energy. At 300 K the fractions of four-fold coordination were slightly lower than those at 100 K in all cases. In general, at 300 K, very high percentages of sp^3 configurations (50%–100%) were obtained near the diamond substrate within the distance of 20 Å with good DLC quality. However, this value dropped to stable values at 30%–50% with further depositions. The quantitative details of the average sp^3 fractions and mass densities for the grown inner stable films of different systems at 100 K and 300 K are shown in Table I. The fractions of sp^3 configuration could not reach very high values at the stable inner films in all cases because the sp^2 bondings are more energetically favorable and stable. The temperature effect was also simulated in the deposition process. sp^3 configurations were observed at lower temperatures than those at higher temperatures, and sp^3 hybridizations were hardly observed at all above 600 K, which agrees with the experiment by Koskinen.[43]

It must be noted that the experimentally deposited ta-C film is much thicker (around 10 times thicker) than the ta-C deposited by simulation. We believe this has an effect on the results, wherein during experimental deposition enough film is deposited to ensure sidewall pressure and form high quality ta-C. Hence the simulated results do not show high enough quality of ta-C when deposited on suspended SWCNT/MWCNT or when they are on substrate.

TABLE I. Average of sp^3 fractions and mass densities at the grown inner stable films, for the cases mentioned above with diamond substrates at 100 K and 300 K.

		100 K		300 K	
Samples		sp^3 (%)	Densities (g/cm^3)	sp^3 (%)	Densities (g/cm^3)
Pure	30 eV	52.6	3.07	40.6	3.00
diamond	40 eV	51.7	3.09	42.4	3.00
	50 eV	61.5	3.15	42.6	3.01
	70 eV	61.1	3.13	52.4	3.06
SWCNT	30 eV	43.0	3.02	27.5	2.92
	40 eV	49.0	3.08	35.6	2.97
	50 eV	51.1	3.10	32.5	2.96
	70 eV	56.3	3.11	26.7	2.92
Nano	30 eV	36.2	2.86	21.9	2.72
foam	40 eV	36.7	2.92	31.6	2.86
	50 eV	44.7	2.96	32.2	2.91
	70 eV	48.1	3.04	36.1	2.92
MWCNT	30 eV	37.6	3.00	26.2	2.89
	40 eV	44.0	3.04	28.0	2.93
	50 eV	64.2	3.16	34.5	2.97
	70 eV	49.8	3.06	38.6	2.99

The fact that our simulations predict the formation of high sp^3 contents at 100 K, but lower at 300 K, while in the room-temperature experiments the sp^3 content is quite high, indicates that the temperature-dependence of the material properties of the potential is not fully correct. Nevertheless, we emphasize that this does not affect the main point of the current work, i.e., the side pressure from the substrate and the two dimensional boundary confinement can lead to the formation of high DLC contents.

Furthermore, at the first peak of overall RDF, the amount of contributions of sp^2 and sp^3 neighbours were roughly proportional to the overall fractions of three-coordinated and four-coordinated atoms in the studied films. When calculated only at sp^2 (or sp^3) sites compared to the overall RDF, a big increase of the sp^2 (or sp^3) neighbours contribution revealed the separation of sp^2 and sp^3 sites, where sp^2 sites were mostly near the surface because of the lack of atoms to form bondings at the top. It is found that the films with higher sp^3 fractions and higher density had relatively more ordered ring analysis results, where the ideal diamond has the most ordered configuration with the most popular six-ring size.

VII. CONCLUSIONS

In conclusion, using experiments and molecular dynamics simulations of C deposition on carbon nanotube and nanofoam systems, we find that high-sp^3-content ($\gtrsim$50 eV) diamond-like carbon films can, under certain conditions, be formed on top of carbon nanostructures. Above 600 K, DLC formation does not occur, in agreement with experiments. Moreover, we found that to get the high sp^3 contents, it is necessary that there is also deposited material on the sides of the nanotubes. Without this condition (i.e., if deposition is carried out on a nanotube system without a substrate close beneath) there is no possibility to maintain a high pressure

and the growing film relaxes to an almost graphitic condition. In other words, the possibility to form a "sidewards pressure" is a prerequisite for forming DLC films on top of the nanostructures. The simulations also showed that for typical DLC cathodic arc deposition energies around 40–70 eV, two carbon layers in the nanotube are destroyed by the deposition, but nanotubes below these layers can remain virtually undamaged.

ACKNOWLEDGMENTS

The sponsorship of the Academy of Finland through the research Project HISCON (Nos. 220911 and 259595) is acknowledged. XPS data collection by Dr. Leena-Sisko Johansson and Dr. Joseph Campbell from Department of Forest Products Technology, Aalto University is acknowledged. Grants of computer time from the Center for Scientific Computing in Espoo, Finland are gratefully acknowledged.

[1]Q. Cao and J. A. Rogers, Adv. Mater. **21**, 29 (2009).
[2]Z. Wu, Z. Chen, X. Du, J. M. Logan, J. Sippel, M. Nikolou, K. Kamaras, J. R. Reynolds, D. B. Tanner, A. F. Hebard *et al.*, Science **305**, 1273 (2004).
[3]B. S. Shim, J. Zhu, E. Jan, K. Critchley, and N. A. Kotov, ACS Nano **4**, 3725 (2010).
[4]A. Kaskela, J. Koskinen, H. Jiang, Y. Tian, X. Liu, T. Susi, M. Kaukonen, A. G. Nasibulin, and E. I. Kauppinen, Carbon **53**, 50 (2013).
[5]H. Schittenhelm, D. B. Geohegan, G. Jellison, A. A. Puretzky, M. J. Lance, and P. F. Britt, Appl. Phys. Lett. **81**, 2097 (2002).
[6]H. Kinoshita, I. Ippei, H. Sakai, and N. Ohmae, Diamond Relat. Mater. **16**, 1940 (2007).
[7]C. Wei, J.-F. Yang, and F.-C. Tai, Diamond Relat. Mater. **19**, 518 (2010).
[8]D. Varshney, B. R. Weiner, and G. Morell, Carbon **48**, 3353 (2010).
[9]N. Sakudo, N. Ikenaga, H. Yasui, and K. Awazu, Thin Solid Films **516**, 4483 (2008).
[10]J. Zhang, Y. Yu, and D. Huang, Solid State Sci. **12**, 1183 (2010).
[11]A. Grill, Diamond Relat. Mater. **8**, 428 (1999).
[12]P. Koidl, A. Bubenzer, and D. Dischler, "Hard carbon coatings for IR-optical components," Proc. SPIE **0381**, 177 (1983).
[13]A. Lettington, P. Koidl, and P. Oelhafen, Proc. Eur. Mater. Res. Soc. Symp. **17**, 359 (1987).
[14]A. Callegari, K. Babich, S. Purushothaman, S. Mansfield, R. Ferguson, A. Wong, W. Adair, D. O'Grady, and V. Chao, Microelectron. Eng. **41**, 107 (1998).
[15]A. H. Lettington, Y. Tzeng, M. Yoshikawa, M. Murakawa, and A. Feldman, *Materials Science Monographs* (Elsevier, New York, 1991), Vol. 703.
[16]A. Evans, J. Franks, and P. Revell, Surf. Coat. Technol. **47**, 662 (1991).
[17]A. Grill, V. Patel, K. Saenger, C. Jahnes, S. Cohen, A. Schrott, D. Edelstein, and J. Paraszczak, in "Symposium H – Low-Dielectric Constant Materials II," edited by H. Treichel, A. C. Jones, A. Lagendijk, and K. Uram (Mater. Res. Soc. Symp. Proc., 1996), p. 155.
[18]A. Grill, V. Patel, and C. Jahnes, J. Electrochem. Soc. **145**, 1649 (1998).
[19]D. McCulloch, D. McKenzie, S. Prawer, A. Merchant, E. Gerstner, and R. Kalish, Diamond Relat. Mater. **6**, 1622 (1997).
[20]A. Kaskela, A. G. Nasibulin, M. Y. Timmermans, B. Aitchison, A. Papadimitratos, Y. Tian, Z. Zhu, H. Jiang, D. P. Brown, A. Zakhidov *et al.*, Nano Lett. **10**, 4349 (2010).
[21]A. G. Nasibulin, A. Kaskela, K. Mustonen, A. S. Anisimov, V. Ruiz, S. Kivisto, S. Rackauskas, M. Y. Timmermans, M. Pudas, B. Aitchison *et al.*, ACS Nano **5**, 3214 (2011).
[22]A. Moisala, A. G. Nasibulin, D. P. Brown, H. Jiang, L. Khriachtchev, and E. I. Kauppinen, Chem. Eng. Sci. **61**, 4393 (2006).
[23]D. Gonzalez, A. G. Nasibulin, S. D. Shandakov, P. Queipo, H. Jiang, and E. I. Kauppinen, Phys. Status Solidi B **243**, 3234 (2006).
[24]A. Iyer, A. Kaskela, L.-S. Johansson, X. Liu, E. I. Kauppinen, and J. Koskinen, J. Appl. Phys. **117**, 225302 (2015).
[25]A. Anders, I. G. Brown, R. A. MacGill, and M. R. Dickinson, J. Phys. D: Appl. Phys. **31**, 584 (1998).
[26]Y. Lifshitz, S. R. Kasi, J. W. Rabalais, and W. Eckstein, Phys. Rev. B **41**, 10468 (1990).
[27]H.-P. Kaukonen and R. M. Nieminen, Phys. Rev. Lett. **68**, 620 (1992).
[28]H. Jäger and K. Albe, J. Appl. Phys. **88**, 1129 (2000).
[29]K. Nordlund (2006), parcas computer code. The main principles of the molecular dynamics algorithms are presented in Refs. 44 and 45. The adaptive time step and electronic stopping algorithms are the same as in Ref. 46.
[30]D. W. Brenner, Phys. Rev. B **46**, 1948 (1992).
[31]D. W. Brenner, in "Symposium T – Atomic Scale Calculations in Materials Science," edited by J. Tersoff, D. Vanderbilt, and V. Vitek (Mater. Res. Soc. Symp. Proc., 1988), Vol. 141, p. 59.
[32]X. Yuan and A. Cormack, Comput. Mater. Sci. **24**, 343 (2002).
[33]S. Doniach and M. Sunjic, J. Phys. C: Solid State Phys. **3**, 285 (1970).
[34]P. T. M. Van Attekum and G. Wertheim, Phys. Rev. Lett. **43**, 1896 (1979).
[35]S. T. Jackson and R. G. Nuzzo, Appl. Surf. Sci. **90**, 195 (1995).
[36]P. Merel, M. Tabbal, M. Chaker, S. Moisa, and J. Margot, Appl. Surf. Sci. **136**, 105 (1998).
[37]A. Herrera-Gomez, Y. Sun, F.-S. Aguirre-Tostado, C. Hwang, P.-G. Mani-Gonzalez, E. Flint, F. Espinosa-Magana, and R. M. Wallace, Anal. Sci. **26**, 267 (2010).
[38]N. Soin, S. S. Roy, S. C. Ray, P. Lemoine, M. A. Rahman, P. D. Maguire, S. K. Mitra, and J. A. McLaughlin, Thin Solid Films **520**, 2909 (2012).
[39]V. Datsyuk, M. Kalyva, K. Papagelis, J. Parthenios, D. Tasis, A. Siokou, I. Kallitsis, and C. Galiotis, Carbon **46**, 833 (2008).
[40]G. Moraitis, Z. Špitalskỳ, F. Ravani, A. Siokou, and C. Galiotis, Carbon **49**, 2702 (2011).
[41]H. J. Berendsen, J. P. M. Postma, W. F. van Gunsteren, A. DiNola, and J. Haak, J. Chem. Phys. **81**, 3684 (1984).
[42]J. F. Ziegler, J. Biersack, and U. Littmark, *The Stopping and Range of Ions in Solids* (Springer, New York, 1985), Vol. 1.
[43]J. Koskinen, J.-P. Hirvonen, and J. Keränen, J. Appl. Phys. **84**, 648 (1998).
[44]K. Nordlund, M. Ghaly, R. S. Averback, M. Caturla, T. D. de la Rubia, and J. Tarus, Phys. Rev. B **57**, 7556 (1998).
[45]M. Ghaly, K. Nordlund, and R. S. Averback, Philos. Mag. A **79**, 795 (1995).
[46]K. Nordlund, Comput. Mater. Sci. **3**, 448 (1995).